 https://doi.org/10.3311/PPci.43725

Periodica Polytechnica Civil Engineering, 70(2), pp. 568–582, 2026

Experimental Study on the Behavior of Reinforced Concrete Columns Under Torsion-axial Combined Loading

Abdulkadir Solak[1*], Mehmet Kamanli[1], Alptug Unal[1], Salih Cengiz[2]

[1] Civil Engineering Department, Faculty of Engineering and Natural Sciences, Konya Technical University, Yeni İstanbul Cad. 363/6, Akademi Mah., 42250 Konya, Türkiye
[2] Construction Department, Vocational School of Technical Sciences, Konya Technical University, Akademi Mah., Yeni İstanbul Cad. 351., 42130 Konya, Türkiye
[*] Corresponding author, e-mail: abdulkadirsolak@ktun.edu.tr

Received: 17 February 2026, Accepted: 22 April 2026, Published online: 01 June 2026

Abstract

The behaviour of columns in irregular structures subjected to seismic effects is significantly influenced by torsional moments arising primarily due to asymmetries in the plan. Torsional moments that occur during earthquakes in irregular buildings have a negative impact on the load-bearing capacity and ductility of columns. Therefore, it is crucial to understand how columns behave when subjected to axial loads and torsional effects in order to ensure safe structural design. Seven column specimens were tested under various axial load ratios. The columns represent residential buildings constructed in earthquake zones prior to 2000 in Turkiye, which do not even meet the seismic code requirements of their construction periods in terms of material properties, longitudinal and transverse reinforcement ratios, and restraint details. This experimental study examined torsional moment capacity, cracking and ultimate rotation values, stiffness loss, ductility and energy dissipation parameters. These were then compared with finite element analyses performed using ABAQUS software. The results reveal that axial load–torsion interaction plays a decisive role in the seismic behaviour of columns, exhibiting a nonlinear character. The findings suggest that there is an optimum axial load range, and that exceeding this range significantly reduces torsional ductility. The study suggests that adequate transverse reinforcement, appropriate detailing and an optimum axial load ratio are crucial for the torsional behaviour of reinforced concrete columns.

Keywords

ABAQUS, column, experimental study, reinforced concrete, seismic behavior, torsion

1 Introduction

In the context of reinforced concrete buildings, the arrangement of load-bearing elements in the plan is a critical factor in ensuring the seismic safety of the structure. The regular placement of load-bearing elements in the plan has been shown to positively affect their behaviour under seismic loads. However, structures that are not designed in accordance with earthquake regulations and have irregular and complex load-bearing mechanisms pose a significant engineering problem worldwide. The materials utilized do not align with contemporary design and performance requirements, owing to the limited regulations and engineering experience that prevailed in the past, as well as the absence of adequate control mechanisms. An analysis of residential buildings constructed in Turkey prior to 2000 reveals common characteristics observed in such structures [1]. These include structures where reinforcement arrangements such as minimum cross-sectional dimensions, material strengths, longitudinal reinforcement ratios, transverse reinforcement spacings, and wrapping conditions (135° stirrup bends or densification zones) do not even meet the regulatory requirements of the relevant period [2–4]. The consequence of the asymmetry in the plan and the eccentricity between the mass and stiffness centre is that larger rotational effects than expected occur in irregular buildings under seismic loading [5–7]. Due to the rotation effect, columns are subjected to torsion moments in addition to pressure, bending, and shear effects. The occurrence of torsion moments has been demonstrated to reduce the load-carrying capacity and ductility of the column [8–10]. Furthermore, when the torsional moment exceeds the cracking moment, torsional stiffness decreases by 90–97% due to the torsional crack that occurs in the column [11, 12]. When torsion crack occurs in the element, plastic hinges form

Cite this article as: Solak, A., Kamanli, M., Unal, A., Cengiz, S. "Experimental Study on the Behavior of Reinforced Concrete Columns Under Torsion-Axial Combined Loading", Periodica Polytechnica Civil Engineering, 70(2), pp. 568–582, 2026. https://doi.org/10.3311/PPci.43725

to ensure equilibrium conditions are maintained. In hyperstatic systems, the occurrence of redistribution is dependent upon the presence of sufficient ductility and rotational capacity, thus allowing for the formation of plastic hinges [13, 14]. Insufficient ductility and rotational capacity are the primary causes of system instability and collapse in the presence of seismic loads. Research conducted both in the academic literature and through field observations has demonstrated that torsional effects in irregular structures have the potential to result in significant damage [6, 15, 16].

In terms of structural behaviour and damage mechanisms, axial load is important in reinforced concrete (RC) columns. Researchers have conducted numerous experimental and numerical studies on the behaviour of RC Columns [17, 18]. Ductile behaviour is dominant in columns at low axial load levels, but as axial load increases ($n > 0.3$), ductility decreases by 30–40% and more brittle damage begins to occur [19]. It has been observed that, under high axial load ($n \approx 0.4$–0.6), the ductility of RC columns decreases by up to 50%, energy consumption decreases, and damage occurs earlier [20].

In recent years, researchers have conducted studies on the torsional behaviour of columns under axial load [8, 10, 21–25]. Studies have shown that the torsional strength of a structure depends on various factors, such as the amount of longitudinal and transverse reinforcement, the properties of the materials used, the shape of the structure and its cross-sectional dimensions [26–29]. In the study conducted by Cengiz [8], the bending behaviour of reinforced concrete columns under axial load and torsion was investigated through an experimental study. It was found that as the torsion effect on the columns increased, the plastic rotation capacity of the elements decreased by approximately 62%. This finding revealed that torsion reduces plastic rotation capacity by creating additional shear stresses in the columns. Ren et al. [23] found that the energy consumption capacity of columns under axial load and torsion decreases by around 10% as the axial load increases. Xu et al. [24] found that increasing the axial load ratio in *L*-section columns from 0.19 to 0.23 reduces torsional capacity by 22.3%. Yu and Shan [25] observed that axial loading generally reduces torsional capacity and cracking, but that appropriate reinforcement and section design can increase ductility. Studies have shown that the damage condition, torsional and bending capacities, and torsional/bending moment ratio of columns are affected, particularly when bending is also present alongside axial load and torsion [8, 21, 30, 31]. Studies have shown that the torsion/bending moment ratio (T/M) plays a critical role in damage mechanisms, ductility, and torsion capacity, in addition to the effects of axial load and bending on behaviour in columns [30–33].

The literature review reveals that studies on combined axial load-torsion loading in columns are typically conducted under monotonic loading conditions. Furthermore, inadequate experimental setups and loading conditions mean that studies in this area are not widespread. In reinforced concrete columns, it is important to understand the effect of torsion on behaviour, as cracking significantly reduces rigidity, affecting load-carrying capacity and ductility by 90–97%.

This study aims to investigate the behaviour of reinforced concrete columns under torsional effects at varying axial load levels. Within this scope, the effect of different axial load levels on torsion behaviour has been examined. The experimental findings were then compared with the finite element model. The study evaluated the damage mechanisms of columns under combined torsion and axial loading conditions, as well as their stiffness characteristics before and after cracking, their energy dissipation capacity and their ductility performance.

2 Experimental program

2.1 Specimen details

In this study, seven columns were produced to investigate the behaviour of columns under torsional effects at varying axial load levels (Table 1). The axial load ratio (n) was considered the primary variable. This is defined as the ratio of the axial load applied to the column (N) to the column's axial load-carrying capacity (N_C). The theoretical axial load-carrying capacity (N_C) was determined by using Eq. (1) [34]. The selected axial load ratios, varying between 0.05 and 0.30, are consistent with the limits stipulated by the Turkish Building Earthquake Code [35].

$$N_C = 0.85 f_{ck} A_c + f_{yk} A_s \tag{1}$$

Torsion was applied cyclically. Moment-rotation, energy consumption and stiffness graphs were plotted for all specimens using the data obtained from the experiments.

Table 1 Properties of the test specimens

Specimen	Axial load ratio (n)	Axial load (kN)
N_0 (Reference)	-	0
N_5	0.05	18
N_{10}	0.10	36
N_{15}	0.15	54
N_{20}	0.20	72
N_{25}	0.25	90
N_{30}	0.30	108

Specimen N_0 was designated as the reference specimen for comparisons between specimens.

The columns were selected to represent the irregular structures found in existing buildings. Accordingly, the specimens were designed with insufficient transverse reinforcement ratio and low concrete compressive strength, and without stirrup reinforcement. The cross-section dimensions were scaled geometrically at a ratio of 1:2. Accordingly, the cross-section dimensions are $b \times h = 150 \times 150$ mm, and the net height of the column is 1500 mm. Torsional effects were applied to the column using a beam with a cross-section of 150 × 200 mm and a length of 550 mm (Fig. 1 (a)). The concrete cover was set at 15 mm for both the column and the beam. The distance between the horizontal loading point on the beam and the centre of the column was determined to be $L = 400$ mm (Fig. 1 (b)). No local damage was observed on the beam during the experiments. The element was firmly connected to the ground using a foundation measuring 800 × 1500 × 500 mm, which was constructed at the bottom of the column (Fig. 1 (a)). A 190 × 190 mm socket cavity was left in the middle of the foundation. The foundation was fixed to the ground using dowels. The 300 mm section of the column was then placed inside the socket. The joint between the column and the foundation was made using a concrete mortar with a compressive strength of 70 MPa. No damage occurred to the mortar joint during the tests.

The columns are designed with 4Ø10 mm longitudinal reinforcement and Ø6/100 mm stirrups. To represent the existing irregular structures, the stirrups have not been densified (Fig. 1 (a)). In line with previous studies, it is accepted that scaled models accurately depict torsion behaviour, and that changes in cross-section dimensions have an acceptable effect on torsional strength [36, 37]. Longitudinal reinforcement of 4Ø10 and Ø6/50 mm stirrups was incorporated in the design of the beams to prevent damage.

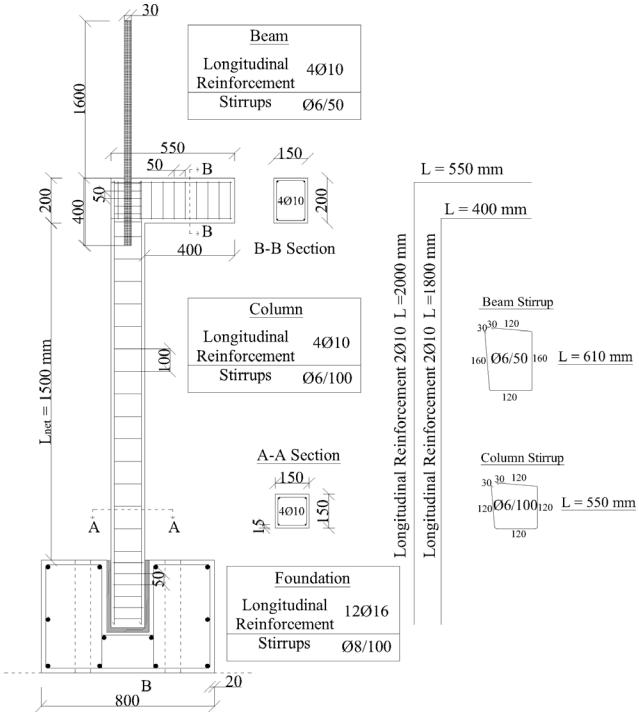

(a)

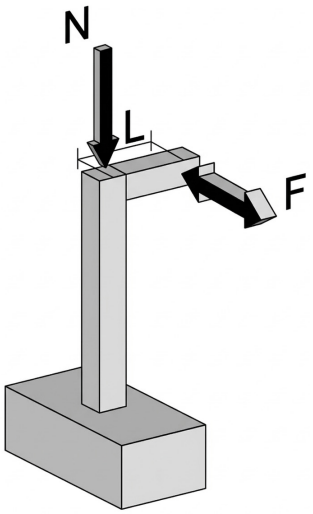

(b)

Fig. 1 Specimen details: (a) Reinforcement; (b) Loading (all dimensions are in mm)

Table 2 Quantities of materials used in concrete mixes (kg/m^3)

Material	Weight
Water	170
Cement	275
Fine aggregate (0–4 mm)	1164
Coarse aggregate (4–12 mm)	758
Superplasticizer	2.50

2.2 Material properties

The concrete used in the test specimens was mixed in accordance with the performance criteria specified in BS EN 206:2013+A1:2016 [38]. Accordingly, the quantities of materials utilized in the mixture are given in Table 2.

Standard tests were conducted for compressive strength and flexural strength in concrete [39, 40]. After 28 days of curing, the mean compressive strength of the concrete cube (150 × 150 × 150 mm) was ascertained to be 25.9 MPa. Utilizing the conversion indicated in Eq. (2), the standard cylinder strength was determined to be 20.31 MPa [41]. The concrete employed in the production process is characterized by a number of mechanical properties, the details of which can be found in Table 3.

Table 3 Mechanical properties of concrete

Feature	Value
Compressive strength (f_{ck})	20.31 MPa
Tensile strength (f_{ctk})	2.10 MPa
Density (d)	2400 kg/m^3
Modulus of elasticity (E)	21200 MPa
Poisson's ratio (v)	0.2

$$f_c' = \left[0,76 + 0,2 \times \log_{10}\left(f_{cu}/19,6\right)\right] \times f_{cu} \quad (2)$$

The average yield stresses for longitudinal reinforcement and stirrups were measured as 408.27 and 387.96 MPa, respectively, and the average ultimate strengths were measured as 510.47 and 454.27 MPa, respectively (Table 4) [28].

2.3 Test setup

An experimental test setup was created for the purpose of investigating the effects of torsional loading on columns in the experimental study (Figs. 2 and 3). In the test setup, a horizontal load was applied to the beam on the column, thereby creating a moment effect in the column ($T = F \times L$). A cyclic torsional moment was thereby created in the column, with the push-pull effect applied to the beam (Fig. 2 (a)). A load cell with a capacity of 500 kN was placed at the extremity of the horizontal loading cylinder in order to calculate the torsional moment (Fig. 2 (a)). In order to prevent damage to the beam and the column-beam connection area due to the effect of horizontal loading, the beam was compressed on both sides with 200 × 700 mm section steel plates. In order to create an axial load on the column, the steel loading beam placed on the column was anchored to the ground. Axial load was created on the column using hydraulic cylinders placed on the loading beam (Fig. 2 (b)). The column was designed to rotate freely under axial load and maintain a load on the specimen through the placement of a rotation bearing system on the column (Fig. 3). A load cell with a capacity of 200 kN was utilized to ascertain the axial load level on the column (Fig. 2 (b)). The axial load was instantly adjusted with ±5 kN accuracy during the loading. In order to prevent bending

Table 4 Mechanical properties of reinforcement

Feature	Value	
	Ø6	Ø10
Modulus of elasticity (E)	203900 MPa	202940 MPa
Yield strength (σ_y)	387.96 MPa	408.27 MPa
Ultimate strength (σ_u)	454.72 MPa	510.47 MPa
Ultimate strain (ε_u)	0.15	0.18
Failure strain (ε_f)	0.31	0.33

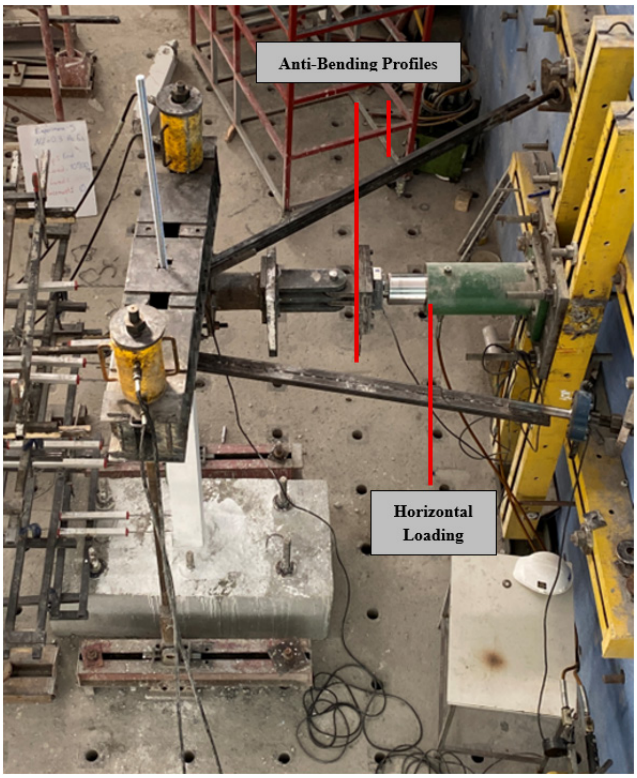

(a)

(b)

Fig. 2 Experimental test setup: (a) Top view; (b) Front view

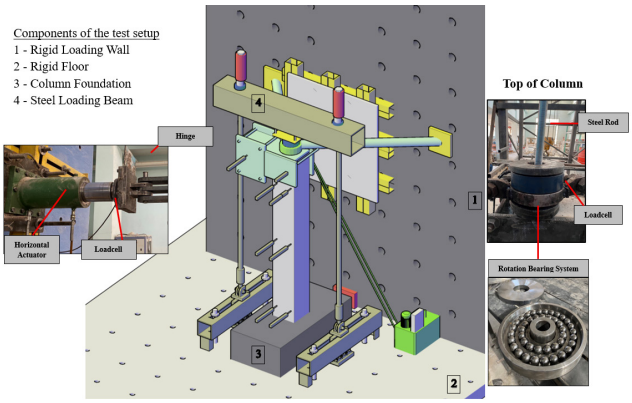

Fig. 3 Experimental test setup (schematic view)

effects caused by horizontal load on the column, a 30 mm diameter steel gijon was placed on the column and fixed to a rigid wall with two cross-placed steel profiles (Fig. 2 (a)). The load and displacement values obtained in the experiments were transferred to a computer environment using a data acquisition system. The configuration of the test apparatus is illustrated schematically in Fig. 3.

In order to ascertain the rotation occurring in the test specimens, one linear potentiometer was placed at the beam end, one on the column axis, and two each in the upper, middle, and lower regions of the column. The glass plates were attached to the points where the linear potentiometers were located. This was to prevent measurement distortion due to rotation and to create a smooth surface. The potentiometer employed to measure displacement in the beam has a maximum displacement capacity of 100 mm in forward-backward cycles. Consequently, the system is capable of achieving a rotation capacity of approximately 0.25 radians within the column. A linear potentiometer was utilised at the base to regulate the displacement of the base during the course of the experiments (Fig. 4).

The axial load (N) acting on the column, the angle of rotation (θ) occurring in the column, and the torsional moment (T) acting on the column were calculated according to the arrangement in Fig. 4 and using Eqs. (3)–(7). The distance L was assumed to be 400 mm.

$$N = LC_V \times 10^{-3}\,(\text{kN}) \tag{3}$$

$$\Delta = LP_{101} - LP_{102} \tag{4}$$

$$\theta = \frac{\Delta}{L} = \frac{\Delta}{400}(rad) \tag{5}$$

$$F = LC_H\,(N) \tag{6}$$

$$T = F \times L = LC_V \times 400 \times 10^{-6}\,(\text{kNm}) \tag{7}$$

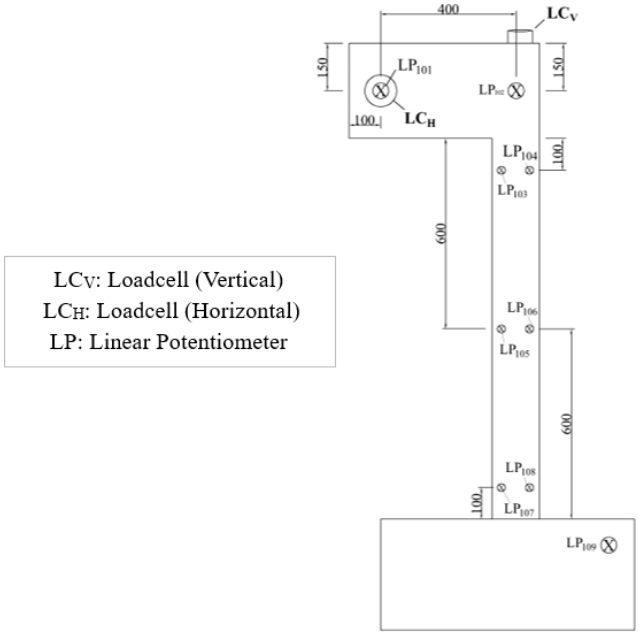

Fig. 4 Placement of measurement elements (all dimensions are in mm)

As demonstrated in the extant literature, the initial crack in the element under torsion typically occurs prior to a rotation value of 0.025 rad [8]. Consequently, the loading up to the cracking point was executed with displacement-controlled increments of 5×10^{-3} rad. Subsequent to this juncture, the experiment was pursued with increments of 0.0125 rad at each loading step. In order to simulate the effects of an earthquake, the loading was applied cyclically at each step, consisting of pushing and pulling (Fig. 5). The experiments were continued until 80% of the maximum capacity was reached.

The moment-rotation diagrams were obtained for each specimen by considering the rotation angle obtained from Eq. (5) and the torsional moment obtained from Eq. (7) corresponding to this angle. The maximum moment occurring in each cycle and the corresponding rotation were determined, and the skeletal curve of the cyclic loading was created. The yield points of the specimens were calculated

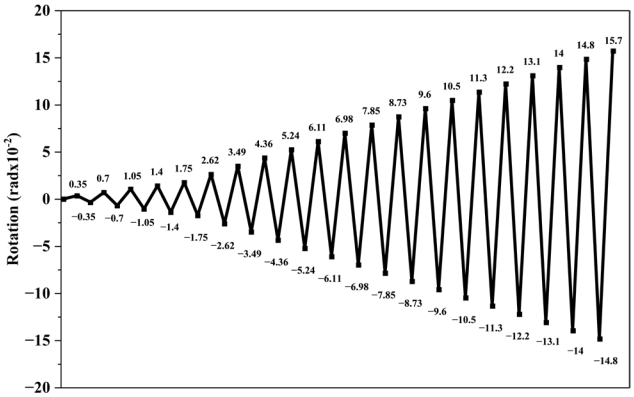

Fig. 5 Loading protocol

according to the First Significant Member Yield (FSMY) criterion (Fig. 6) [42]. The torsional ductility coefficient (μ_θ) was defined as the ratio of the final rotation angle θ_{max} to the yield rotation angle θ_y (Eq. (9)). Furthermore, the torsional stiffness of the specimens was determined using the slope of the moment-rotation graph for each cycle (Eq. (8)).

$$k = \frac{T}{\theta}(\text{kNm/rad}) \tag{8}$$

$$\mu_\theta = \frac{\theta_u}{\theta_y} \tag{9}$$

The energy consumption capacity of each test specimen was determined by calculating the area under its load-displacement curve. Energy consumption has been calculated cumulatively, taking into account the areas of all torsion-moment-rotation cycles obtained up to migration. The unloading - reloading behaviour has not been incorporated into the energy calculation (Eqs. (10)–(12)). Total energy consumption was determined using Eq. (13) (Fig. 7) [43].

$$\theta_i = \theta_2 - \theta_1 \tag{10}$$

$$T_{i,avg} = (T_1 + T_2)/2 \tag{11}$$

$$E_i = \theta_i \times T_{i,avg} \tag{12}$$

$$E = \sum E_i + E_{i+1} + E_{i+2} + \ldots \tag{13}$$

2.4 Finite Element (FE) model

In numerical analyses, the mechanical behaviour of concrete was simulated using the Concrete Damage Plasticity (CDP) model in the ABAQUS 2021 program [44]. The CDP model is predicated on the assumption that it is possible to account for the nonlinear behaviour of concrete, crack propagation, and plastic deformations, and that this enables the model to produce realistic results. The CDP model is predicated on the premise that stress-strain relationships can be defined under both compression and tension, thereby ensuring accurate prediction of column behaviour under the combined effects of axial load and torsion. Stress-strain diagrams for the defined concrete and reinforcement are provided in Fig. 8. In the Concrete Damage Plasticity (CDP) model, which is utilized to simulate the inelastic behaviour of concrete, the parameters delineating the plastic flow surface and volumetric change characteristics of the material have been determined based on extant literature references. In this context, the expansion angle (ψ), which represents the volumetric expansion of concrete under shear, has been accepted as 36° to reflect the effect of medium-level confinement. The value of eccentricity was set at 0.1 and the ratio of biaxial to uniaxial compressive strength (f_{bo}/f_{co}) was established at 1.16, a figure that has been extensively documented in the extant literature [45]. The *K* parameter, which represents the ratio of the second stress invariant in the tensile meridian to the compressive meridian, was selected as 0.667. The viscosity parameter was maintained at a level that would not compromise the accuracy of the results (0.0005) [46]. The damage variables representing stiffness degradation in the material were defined as follows: For compressive damage (d_c), the linear elastic limit of concrete was set to 0.4 f_c and tensile damage (d_t) was considered to be 0.90, based on the decrease in stiffness after cracking [47]. Concrete fracture energy (G_f) was calculated according to Eq. (14) and defined as 129.2 N/m [48].

$$G_f = 73.f_{cm}^{0.18} \tag{14}$$

The scaled models were derived from the experimental study, with a 1:1 ratio employed to ensure fidelity in the replication process. In the modelling process, the material properties obtained in the experimental study were defined. The material parameters are summarized in Tables 2 and 3 [28]. In accordance with the experimental study, the longitudinal reinforcement consists of 4Ø10 bars and Ø6/100 mm shear reinforcement is placed along the column length (Fig. 9). All reinforcements were modelled as bar elements, with appropriate cross-section assignments. Finally, the torsion moment-rotation envelope curve obtained from numerical study was compared with the envelope curves obtained from the experimental study.

In order to simplify the numerical model and optimize computational time, the foundation and the top loading beam were not physically modeled as solid elements. Instead, boundary conditions were applied to represent the experimental setup. A fixed boundary condition was assigned to the bottom surface of the column to simulate the rigid foundation

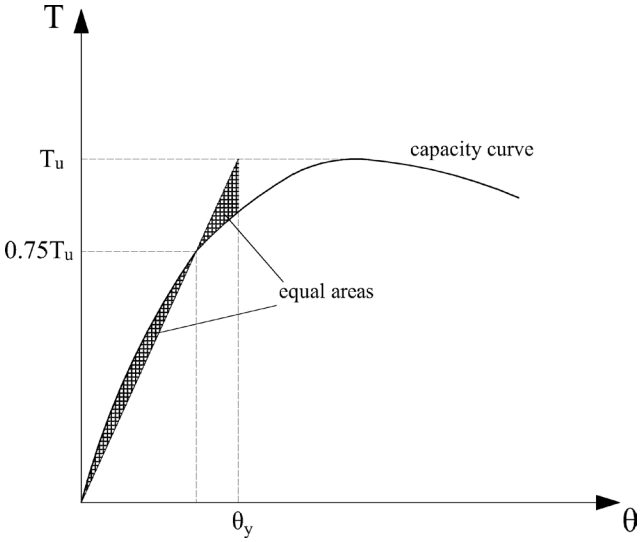

Fig. 6 The definition of yield point for a single element [42]

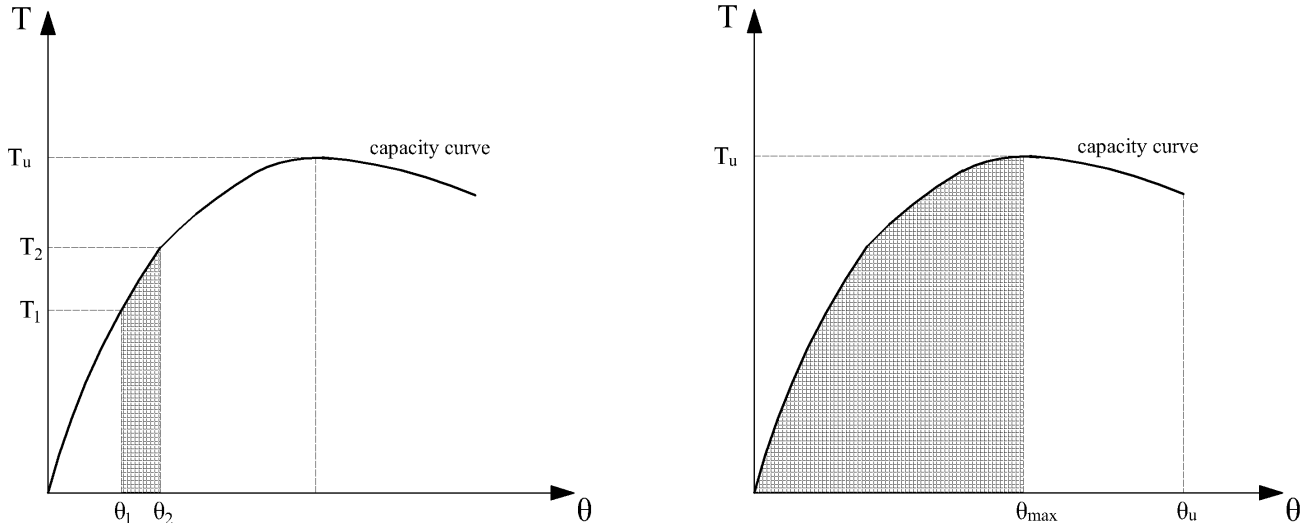

Fig. 7 Energy consumption calculation: (a) cycle; (b) cumulative[43]

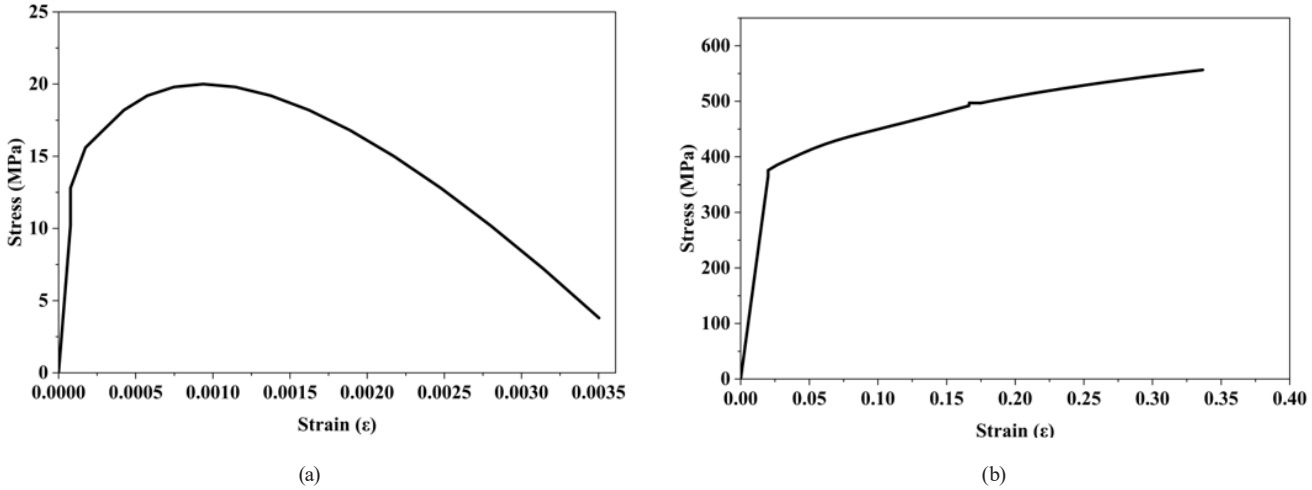

Fig. 8 Stress-strain relationships: (a) CDP model; (b) reinforcement model

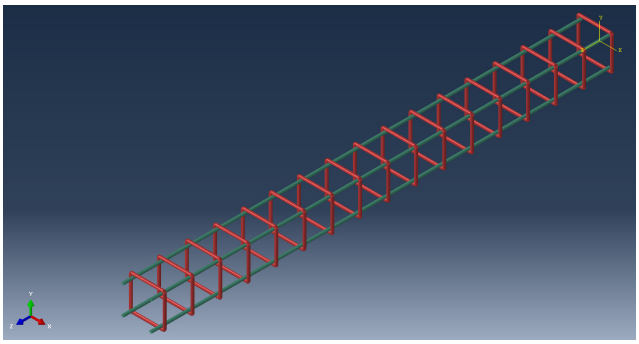

Fig. 9 Reinforcement of numerical model

connection. At the top surface, a kinematic coupling was defined to a reference point where the axial load and cyclic torsional moments were directly applied.

3 Test results

3.1 Torsional moment-rotation angle relations

$T_{-\theta}$ diagrams for cyclic loading were created for each specimen using data obtained from the experimental study (Fig. 10). The envelopes of the specimens were created using the maximum torsional moment in each cycle and the corresponding rotation angles (Fig. 11). Furthermore, the critical points of the specimens' torsional behaviour and the torsional ductility factors for each specimen were determined (Table 5).

The torsional cracking moment was measured as 2.85 kNm in the reference specimen during compression and −1.93 kNm during tension. In the specimens examined, the torsion cracking moment exhibited an increase in both compression and tension cycles in comparison to the reference specimen. In comparison with the reference specimen, the cracking moment exhibited a 77% increase in the N_{25} specimen during compression cycles. As the tension increased, the cracking moment exhibited a 186% increase in the N_{20} specimen in comparison with the reference specimen. In the N_{30} specimen, where the axial load reached 30%, the increase in cracking moment was 33–42% compared to the reference specimen.

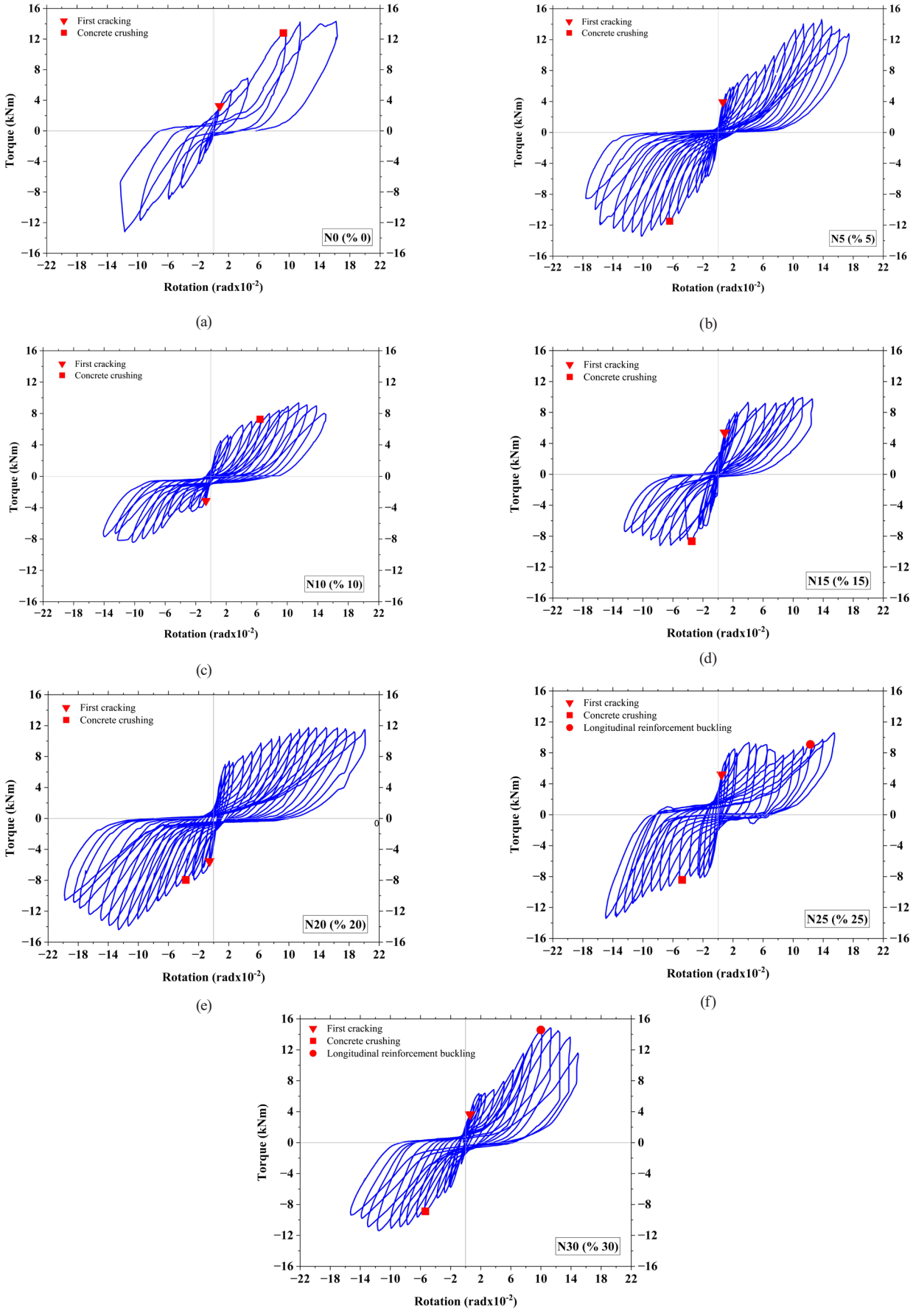

Fig. 10 Cyclic loading curve for specimens: (a) N0 (0%); (b) N5 (5%); (c) N10 (10%); (d) N15 (15%); (e) N20 (20%); (f) N25 (%25); (g) N30 (%30)

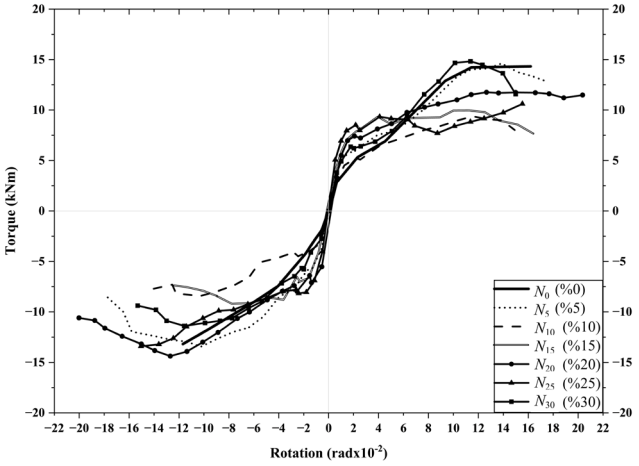

Fig. 11 Skeleton curves of all the specimens

At the moment of cracking, the rotation angle of all specimens was measured between 0.48 × 10^{-2} rad and 0.90 × 10^{-2} rad. The change in the moment capacity of the specimens at the moment of cracking compared to the reference specimen was measured between −8% and 186%. The rotation values occurring in the specimen up to the moment of cracking varied between −25% and 57.9% in comparison with the reference specimen. A more pronounced change was observed in the cracking moment compared to the rotation amount at the moment of cracking. This phenomenon suggests that axial load increases the rigidity of the section prior to the onset of cracking.

The maximum torsional moment was measured at approximately 14 kNm in specimens N_0 and N_5, while it was measured at approximately 9 kNm in specimens N_{10}, N_{15}, and N_{25}. In comparison with the other specimens, both the maximum moment capacity and the ductility ratio were measured at their lowest level in specimen N_{10}. It is assumed that the capacity diminished in specimens N_{10}, N_{15}, and N_{25} due to shear stresses caused by torsion, resulting in crushing.

Torsion capacity of specimen N_{30} was measured at 14.83 kNm in the push cycle and 11.40 kNm in the pull cycle. In the N_{30} specimen, where the axial load reached 30%, it is assumed that the capacity increased due to the increased compression effect. However, upon reaching the maximum torsion point in the specimen, a sudden and brittle fracture occurred. Furthermore, the occurrence of torsion was identified in the longitudinal reinforcement.

The torsional stiffness after cracking is higher in specimens N_0, N_5, and N_{30} compared to other specimens. In comparison to other specimens, N_{20} demonstrates a higher capacity for rotation. In this specimen, there was a 25.6% increase in the positive direction and a 71.3% increase in the negative direction compared to the reference specimen. It is assumed that in the N_{20} specimen, the axial load effect delays crack formation by strengthening the load transfer mechanisms between concrete and reinforcement (e.g. crack edge friction, adhesion, and reinforcement contribution), thereby creating greater rotation capacity. In the N_{25} and N_{30} specimens, the rotation capacity decreased due to the increased compression effect. The present study determined that the rotational capacity of columns under axial load and torsion effects is not linear and decreases when a critical threshold (between 20% and 25% in this study) is exceeded. The 20%–25% axial load ratio was identified as the optimal range for specimens under torsion effects.

3.2 Stiffness

The torsion behaviour of the specimens was evaluated by plotting stiffness-rotation graphs for each loading cycle. As demonstrated in Fig. 12, upon the onset of cracking, there was a decline in the initial torsion stiffness values. These values ranged from 2 to 10 kNm/rad, and upon the occurrence of said cracking, they decreased to 0–2 kNm/rad. Consequently, the stiffness of all specimens decreased by approximately 90% after cracking. The loss of stiffness after cracking is consistent with the results of studies in the literature [11, 12].

Table 5 Mechanical characteristics of specimens

Specimen	Crack moment (kNm)		Crack rotation (rad × 10^{-2})		Yield moment (kNm)		Yield rotation (rad × 10^{-2})		Max torsion (kNm)		Ultimate rotation (rad × 10^{-2})		Rotation ductility coefficient (μ_θ)	
	(+)	(−)	(+)	(−)	(+)	(−)	(+)	(−)	(+)	(−)	(+)	(−)	(+)	(−)
N_0	2.85	−1.93	0.64	−0.57	5.34	−4.26	2.32	−1.87	14.31	−13.19	16.20	−11.68	6.98	6.25
N_5	3.92	−3.77	0.64	−0.57	5.77	−5.75	1.57	−1.61	14.61	−13.43	17.59	−17.71	11.20	11.00
N_{10}	2.63	−3.44	0.50	−0.90	5.25	−4.49	2.18	−2.44	9.38	−8.42	14.92	−14.03	6.84	5.75
N_{15}	3.74	−4.16	0.48	−0.78	7.86	−6.65	2.23	−1.55	9.22	−9.76	16.45	−12.39	7.37	7.99
N_{20}	3.36	−5.53	0.62	−0.54	7.22	−7.96	2.55	−3.70	11.73	−14.38	20.36	−20.01	7.98	5.40
N_{25}	5.05	−4.02	0.50	−0.50	7.96	−7.81	2.07	−2.58	9.33	−9.89	15.35	−15.04	7.41	5.82
N_{30}	3.79	−2.74	0.64	−0.57	6.36	−5.78	1.75	−1.99	14.83	−11.40	14.99	−15.32	8.56	7.70

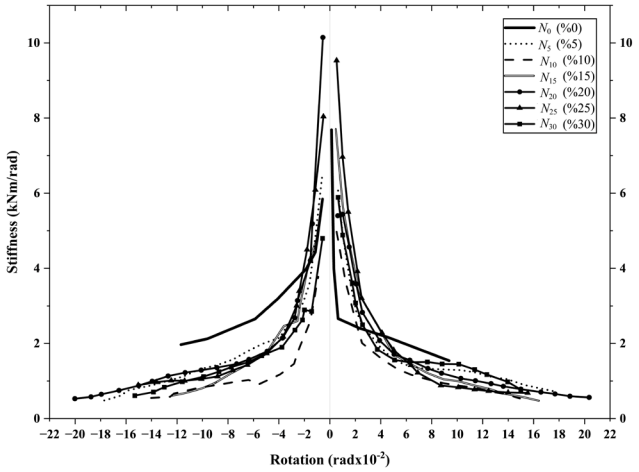

Fig. 12 Stiffness of all specimens

The initial torsional stiffness of the N_0 and N_{10} specimens was measured as 3 kNm/rad. The initial stiffness values of the N_{15}, N_{20}, and N_{25} specimens, which had higher axial loads, reached 7.8, 9.7, and 9.5 kNm/rad, respectively. This finding indicates that the axial load enhances the stiffness and load-bearing capacity of the concrete prior to the onset of cracking. However, under high axial loads, brittle damage mechanisms such as buckling of longitudinal reinforcement and crushing of the core concrete may occur in the specimens. The crushing of the core concrete and buckling of the reinforcement observed in the N_{25} and N_{30} specimens lend support to this assessment.

In specimens with high axial loads (N_{20} and N_{25}), the loss of stiffness occurs much more abruptly. In specimens with low axial loads (N_5) or no load (N_0), due to their low initial stiffness, the decrease in stiffness is at a lower level. As the rotation amount approached 2 × 10^{-2} rad in all specimens, the stiffness was approximately 2 kNm/rad. As the rotational amount increased (after 12 × 10^{-2} rad), only the N_0 specimen was damaged and the experiment was terminated. Irrespective of the axial load ratio, it has been observed that the stiffness of all other specimens falls below 1 kNm/rad.

3.3 Energy consumption

The experimental findings demonstrate that axial load exerts a two-phase effect on energy consumption under torsional loading conditions. The energy consumption measured in specimens N_0 and N_5 was 7–8 kNm, while it was measured as 30 kNm in specimen N_{10} and 55 kNm in specimen N_{15}. The energy consumption of specimens N_{20} and N_{25} were measured at 75 kNm and 110 kNm, respectively. In these specimens, there was an increase of approximately 10 and 14.7 times compared to the reference specimen. In the N_{30} specimen, energy consumption increased sevenfold compared to the reference specimen; however, a decrease of approximately 40% was observed compared to N_{25}. This phenomenon is believed to be the result of the regional crushing of the concrete. Consequently, the axial load-torsion interaction is non-linear in terms of energy consumption. At the optimum axial load effect (approximately 20–25% for the specimens in this study), the torsion capacity and energy consumption capacity are higher. When the optimum axial load level is exceeded (N_{30}), the rotation capacity is reduced due to the compression effect in the specimen. Consequently, the energy consumption capacity is reduced. This finding underscores a pivotal consideration for the design of columns that are susceptible to torsional effects. Consequently, in addition to providing adequate shear reinforcement and appropriate detailing, the optimal axial load range must be taken into account in the design (Fig. 13).

3.4 Damage mechanism of columns

A comprehensive review of extant literature and experimental findings suggests that the location of damage in columns under torsion is a critical parameter. In specimens N_0 and N_{20}, cracks manifested predominantly in the lower region, while in other specimens, they initiated in the middle region. Furthermore, in all specimens, damage progressed from the column edges towards the corners. In all specimens, damage was observed to develop in the regions where the initial cracks appeared (Fig. 14). With a decrease in torsional stiffness, brittle failures occurred in the specimens, and as the axial load level increased, buckling in the longitudinal reinforcement and crushing in the core concrete were observed (N_{25}, N_{30}). The findings of this study demonstrate a direct correlation between the loss of stiffness and the sudden reduction in capacity, with the presence of a high axial load having a propensity to expedite the loss of ductility.

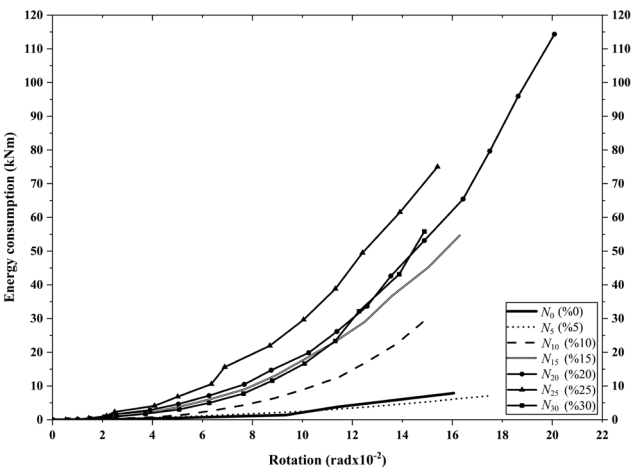

Fig. 13 Energy consumption of all specimens

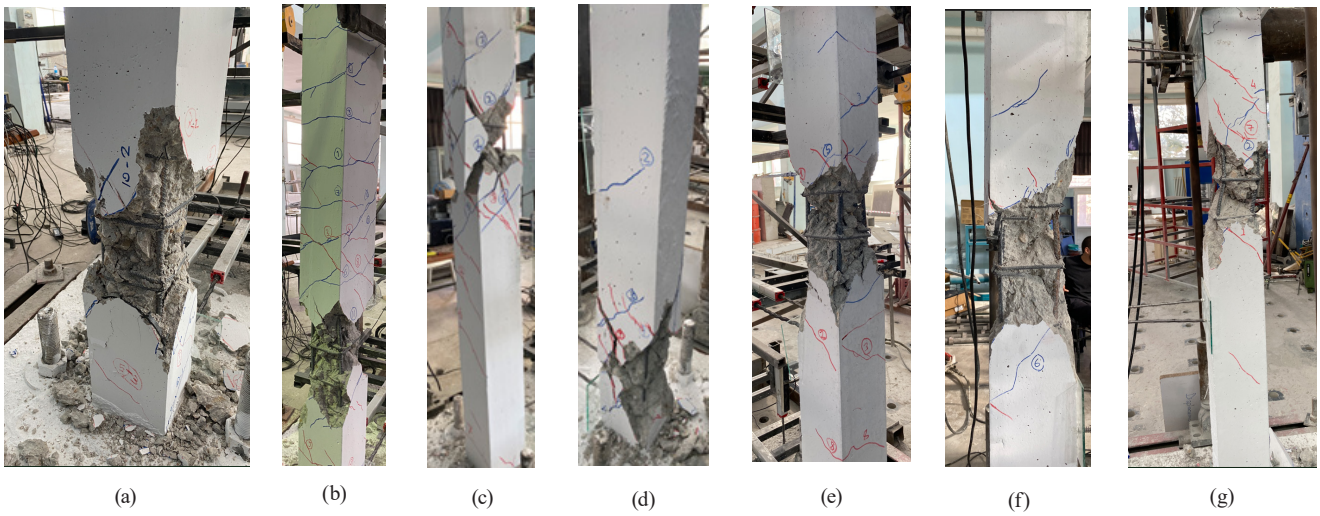

(a) (b) (c) (d) (e) (f) (g)

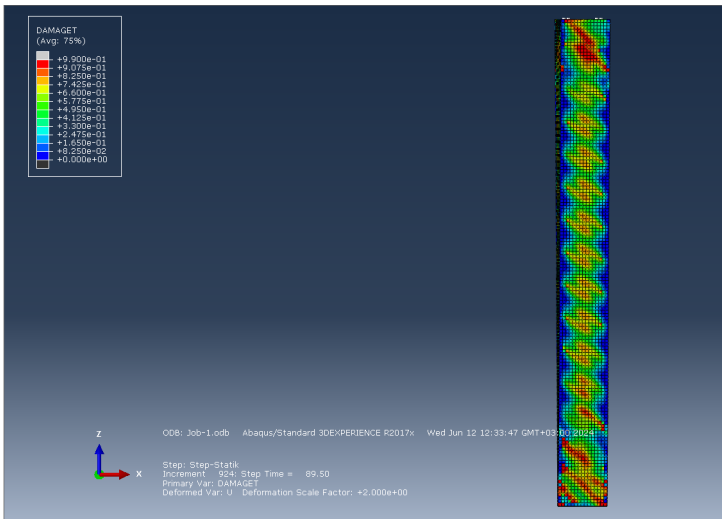

(h)

Fig. 14 Comparison of damaged specimens: (a) N_0 (0%); (b) N_5 (5%); (c) N_{10} (10%); (d) N_{15} (15%); (e) N_{20} (20%); (f) N_{25} (%25); (g) N_{30} (%30); (h) FE Model

The determination of the plastic hinge length (L_p) is of critical importance in the evaluation of the seismic performance of reinforced concrete columns. The length of the plastic hinge has been determined on the basis of measurements of the crack concentration zone. In specimen N_{10}, the plastic hinge formed at a comparatively reduced length and within a circumscribed area, while in other specimens, plastic hinge lengths exhibited variability (Table 6). This situation indicates that the axial load level plays a critical role not only in torsional stiffness but also in the propagation of damage and the formation of plastic hinge regions. In the extant literature, L_p=0.5h is generally accepted for the plastic hinge length [49, 50]. The experimental study revealed that the lengths of the plastic hinges obtained were greater than the accepted value in literature. In the extant literature, the expression L_p = 0.5h is accepted in numerous publications and regulations. However, it should be noted that this expression does not consider the loading conditions of the element, nor the effect of transverse reinforcement. [49, 50]. It has been determined that the values of L_p obtained are in excess of the commonly accepted values. This is due to the fact that the torsion effect is effective throughout the entire element, rather than in a specific region of the element, and due to the insufficient effect of the wrapping. In actual conditions, it has been observed that loading

Table 6 Plastic hinge lengths and locations

Specimen	Plastic hinge length L_p (mm)	L_p/h	Position on column
N_0 (Reference)	300	2.0	Lower-mid of the column
N_5	270	1.8	Lower-mid of the column
N_{10}	150	1.0	Mid of the column
N_{15}	340	2.3	Lower of the column
N_{20}	240	1.6	Mid of the column
N_{25}	300	2.0	Mid of the column
N_{30}	270	1.8	Mid of the column

conditions, axial load level and transverse reinforcement ratio also affect the determination of the plastic hinge length.

3.5 FE results

The moment-rotation diagrams obtained using the finite element method were then compared with the diagrams obtained in the experimental study (Fig. 15). In the numerical analysis, it was observed that the load-bearing capacity decreased in proportion as the torsion in the column increased. In columns under torsion, greater rotation occurs in the 10–25% axial load range, while lower torsion moments are exhibited in columns at this axial load level. Upon examination of Fig. 15, it is evident that the initial stiffness of specimens N_0 and N_5 exceeds that of the other specimens. It is evident that the stiffness is reduced in specimens that are subjected to an axial load of 10% and above. Furthermore, specimens N_{20}, N_{25}, and N_{30} demonstrated a higher degree of ductile behaviour in comparison to the other specimens. The percentage error rates, based on the mechanical properties obtained in the numerical analysis and experimental data, are given in Table 7. The yield moment values exhibited an error of almost 2 times in specimens N_0, N_5, and N_{10}. The results for the other specimens are closely aligned with the experimental study. The mean percentage error in the maximum moment and ultimate rotation values is 5.91% and 1.93%, respectively. The 20–50% error in rotation ductility factors can be attributed to inaccuracies in the numerical estimation of yield stress, with specimen N_{20} showing the highest error.

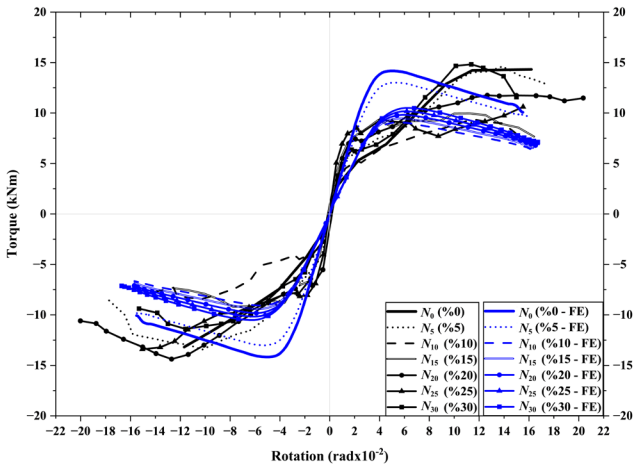

Fig. 15 Comparison of experimental and numerical results

In columns subjected to axial load and torsion, experimental and numerical analyses revealed 45° diagonal cracks originating at the corners and converging at the edges. In the experimental phase, damage was observed in the lower and middle regions of the column; however, in the numerical study, the damage became more pronounced in the upper and lower parts of the columns (Fig. 15). In the experimental study, the hinging continued at the point of initial damage to the column, with no progression of damage observed in other regions. The lengths of the plastic hinges were found to be consistent with the experiments and the literature. Despite the fact that reinforced concrete specimens possess a heterogeneous structure, numerical analyses assume homogeneous material. Consequently, while localized damage is evident in the experimental specimen, the analysis results demonstrate a propagation of damage across the specimen.

4 Conclusions

The present study investigates the behaviour of reinforced concrete columns under different axial load levels and torsional effects, both experimentally and numerically. The following aspects are evaluated in the ensuing discussion: cracking moments under torsion, torsional moment carrying capacities, rotation amounts, ductility, and damage conditions.

Table 7 Comparison of numerical and experimental results

Specimen	Yield moment (kNm)			Yield rotation (rad × 10^{-2})			Max torsion (kNm)			Ultimate rotation (rad × 10^{-2})			Rotation ductility coefficient (μ_θ)		
	Exp. (Avg)	FE	Errors (%)	Exp. (Avg)	FE	Errors (%)	Exp. (Avg)	FE	Errors (%)	Exp. (Avg)	FE	Errors (%)	Exp. (Avg)	FE	Errors (%)
N_0	4.8	10.1	110.42	2.10	1.62	−35.08	13.75	14.17	3.05	13.94	15.51	11.26	6.62	9.57	44.62
N_5	5.76	10.75	86.63	1.59	1.73	8.81	14.02	13.02	−7.13	17.65	15.84	−10.25	11.1	9.16	−17.51
N_{10}	4.87	6.93	42.30	2.31	1.61	−30.30	8.9	9.07	1.91	14.48	15.68	8.32	6.30	9.74	54.71
N_{15}	7.26	7.4	2.00	1.89	1.73	−8.47	9.49	9.45	−0.42	14.42	15.67	8.67	7.68	9.06	17.94
N_{20}	7.59	7.25	−4.48	3.13	1.65	−47.20	13.05	9.82	−24.78	20.19	16.53	-18.11	6.69	10.02	49.75
N_{25}	7.89	7.05	−10.59	2.33	1.57	−32.47	9.61	10.17	5.83	15.20	15.71	3.39	6.615	10.01	51.27
N_{30}	6.07	7.4	21.91	1.87	1.65	−11.76	13.12	10.50	−19.88	15.16	16.71	10.26	8.13	10.13	24.57

It was demonstrated that the torsional cracking moment exhibited an increase in proportion to the axial load. At low axial load levels, the amount of rotation increased while the load-carrying capacity decreased. This finding suggests that columns supporting medium axial loads are of greater importance in terms of torsion.

It was established that the initial stiffness was similar in all specimens. Furthermore, it was demonstrated that the stiffness after cracking decreased by approximately 90%. It was demonstrated that an increase in axial load resulted in enhanced stiffness prior to the onset of cracking. However, subsequent to the occurrence of cracking, the material exhibited brittle damage. Observations made at elevated axial load levels revealed instances of longitudinal reinforcement buckling and concrete crushing. While the initial increase in axial load resulted in enhanced stiffness, it also led to a more precipitous decline. However, at high rotation values, all specimens attained comparable low residual stiffness levels (below 1 kNm/rad).

It has been determined that axial load exerts a two-stage effect on energy consumption. It was observed that the energy consumption capacity of specimens N_{10}, N_{15}, and N_{20} increased by 10–15 times in comparison with the reference specimen. However, the energy consumption of specimens N_{25}–N_{30} increased by 5.5–8 times, a consequence of a loss of ductility. This situation demonstrates that the axial load-torsion interaction is non-linear and that the optimum axial load range (20–25%) is significant in terms of design.

The progression of damage was typically observed to occur in the areas where initial cracks had formed; in certain specimens, this damage was observed to be concentrated in the lower region, while in other specimens, it was concentrated at a medium height. As the axial load increased, brittle fractures and reinforcement buckling were observed. In both experimental and numerical investigations, 45° diagonal cracks were observed, originating at the edges of the columns and converging at the corners. The plastic hinge lengths ranged from h to 2.3h, and the bending plastic hinge assumption in the literature was observed to be valid, with the hinge length increasing with the effect of torsion. From a design perspective, it should be noted that damage can concentrate not only at the column base but also in the middle regions. In order to mitigate this, ductility should be increased with sufficient detailing and dense reinforcement arrangements in critical regions.

Numerical analyses demonstrate a decrease in torsional capacity with increasing axial load. Furthermore, specimens exhibit greater ductility at axial load levels of 10–25%. The analysis results are consistent with the experimental study in terms of initial stiffness and moment capacity. However, discrepancies have been observed in the moment capacity at the yield point and post-yield stiffness of the specimens. In the experimental study, the profiles employed for the prevention of bending subsequent to damage occurrence in the specimen also exerted an influence on the actual behaviour of the specimens due to load carrying under cyclic loading. Consequently, experiments should be conducted with loading combinations that incorporate bending.

In numerical models, damage occurred in a distributed manner along the column. This was due to the assumption of homogeneous material.

Consequently, in columns with inadequate material properties, deficient in detailing, and failing to meet even the seismic code requirements of the period with regard to design details; moderate axial loads increased torsional ductility and energy absorption capacity, while excessive axial loads caused brittleness and loss of ductility in the concrete. It was determined that the loss of rigidity after cracking was significant.

In light of the experimental findings obtained in this study, it is imperative to enhance the torsional ductility and strength of columns subjected to torsional effects. A review of the extant literature suggests that torsional ductility can be enhanced through the implementation of appropriate stirrup arrangements and diverse reinforcement methodologies. Furthermore, it is imperative for designers to consider that plastic hinges under torsion can form not only at the base of the column but also in the middle regions.

Acknowledgement

This study is based on the findings of the first author's MSc thesis. The study was supported by Konya Technical University BAP coordination office with the project number 221004021. The data that support the findings of this study are available on request from the corresponding author.

References

[1] Aydogdu, H. H., Ilki, A. "Case study for a performance based rapid seismic assessment methodology (PERA2019) based on actual earthquake damages", Bulletin of Earthquake Engineering, 22(4), pp. 1965–1999, 2024. https://doi.org/10.1007/s10518-023-01841-5

[2] Kamanli, M., Döndüren, M. S., Çogurcu, M. T., Kekec, B, Unal, A., …, Torun, S. "February 6, 2023 Kahramanmaras Earthquakes; Hatay (Türkiye)", Egitim Yayinevi, 2023. ISBN: 9786256489394

[3] Demirel, I. O., Yakut, A., Binici, B. "Seismic performance of mid-rise reinforced concrete buildings in Izmir Bayrakli after the 2020 Samos earthquake", Engineering Failure Analysis, 137, 106277, 2022. https://doi.org/10.1016/j.engfailanal.2022.106277

[4] Kazaz, İ., Avşar, Ö., Dilsiz, A. "Importance of building inspection on the seismic response of a severely damaged RC structure during the February 6, 2023, Kahramanmaraş earthquake sequence", Engineering Failure Analysis, 162, 108410, 2024. https://doi.org/10.1016/j.engfailanal.2024.108410

[5] Chandler, A. M. "Building damage in Mexico City earthquake", Nature, 320, pp. 497–501, 1986. https://doi.org/10.1038/320497a0

[6] Gokdemir, H., Ozbasaran, H., Dogan, M., Unluoglu, E., Albayrak, U. "Effects of torsional irregularity to structures during earthquakes", Engineering Failure Analysis, 35, pp. 713–717, 2013 https://doi.org/10.1016/j.engfailanal.2013.06.028

[7] Guéguen, P., Astorga, A. "The Torsional Response of Civil Engineering Structures during Earthquake from an Observational Point of View", Sensors, 21(2), 342, 2021. https://doi.org/10.3390/s21020342

[8] Cengiz, S. "The Effect of Axial Load Ratio and Torsional Moment on the Flexural Capacity of Reinforced Concrete Columns", PhD Thesis, Konya Teknik Üniversitesi, 2025.

[9] Kan, C. L., Chopra, A. K. "Elastic earthquake analysis of torsionally coupled multistorey buildings", Earthquake Engineering & Structural Dynamics, 5(4), pp. 395–412, 1977. https://doi.org/10.1002/eqe.4290050406

[10] Nie, J. G., Wang, Y. H., Fan, J. S. "Experimental research on concrete filled steel tube columns under Combined compression-bending-torsion cyclic load", Thin-Walled Structures, 67, pp. 1–14, 2013. https://doi.org/10.1016/j.tws.2013.01.013

[11] Ersoy, U., Özcebe, G., Canbay, E. "Betonarme Cilt 1, Davranış ve Hesap İlkeleri" (Reinforced Concrete 1, Principles of Behavior and Design), Evrim Yayınevi - Akademik Kitapları, 2019. (in Turkish) ISBN 9789755032399

[12] Lampert, P. "Postcracking Stiffness of Reinforced Concrete Beams in Torsion and Bending", ACI Symposium Publication, 35, pp. 385–433, 1973.

[13] ACI "ACI CODE-318-19(22) Building Code Requirements for Structural Concrete and Commentary", ACI Committee, Farmington Hills, MI, USA, 2022.

[14] CEN "Eurocode 2: Design of Concrete Structures – Part 1-1: General Rules and Rules for Buildings (BS EN 1992-1-1:2004)", European Committee for Standardization, Brussels, Belgium, 1992.

[15] Attarchian, N., Kalantari, A., Sarvghad Moghadam, A. "Developing a new procedure for evaluating the ductility capacity of rectangular RC piers subjected to biaxial flexural loadings", Engineering Structures, 172, pp. 187–200, 2018. https://doi.org/10.1016/j.engstruct.2018.05.108

[16] Özmen, G., Girgin, K., Durgun, Y. "Torsional irregularity in multistory structures", International Journal of Advanced Structural Engineering (IJASE), 6(4), pp. 121–131, 2014. https://doi.org/10.1007/s40091-014-0070-5

[17] Dai, K. Y., Lu, D. G., Yu, X. H. "Experimental investigation on the seismic performance of corroded reinforced concrete columns designed with low and high axial load ratios", Journal of Building Engineering, 44, 102615, 2021. https://doi.org/10.1016/j.jobe.2021.102615

[18] Rodrigues, H., Varum, H., Arêde, A., Costa, A. "Behaviour of reinforced concrete column under biaxial cyclic loading—state of the art", International Journal of Advanced Structural Engineering, 5(1), 4, 2013. https://doi.org/10.1186/2008-6695-5-4

[19] Park, R.,Paulay, T. "Reinforced Concrete Structures", John Wiley & Sons, 1975. ISBN 9780471659174 https://doi.org/10.1002/9780470172834

[20] Sheikh, S. A., Uzumeri, S. M. "Strength and Ductility of Tied Concrete Columns", Journal of the Structural Division, 106(5), pp. 1079–1102, 1980. https://doi.org/10.1061/JSDEAG.0005416

[21] Attarchian, N., Attari, N. K., A., Waezi, Z. "Experimental Investigation of the Seismic Performance of Rectangular Reinforced Concrete Columns Subjected to Combined Flexure-torsion Cyclic Loading", Journal of Earthquake Engineering, 26(8), pp. 3954–3976, 2022. https://doi.org/10.1080/13632469.2020.1822225

[22] Cao, X., Wu, L., Li, Z. "Behaviour of steel-reinforced concrete columns under combined torsion based on ABAQUS FEA", Engineering Structures, 209, 109980, 2020. https://doi.org/10.1016/j.engstruct.2019.109980

[23] Ren, Q. X., Han, L. H., Hou, C., Tao, Z., Li, S. "Concrete-encased CFST columns under combined compression and torsion: Experimental investigation", Journal of Constructional Steel Research, 138, pp. 729–741, 2017. https://doi.org/10.1016/j.jcsr.2017.08.016

[24] Xu, D., Yang, Y., Chen, Z. "Experimental Study and Damage Model on the Seismic Behavior of Reinforced Concrete L-Shaped Columns under Combined Torsion", Applied Sciences, 10(19), 7008, 2020. https://doi.org/10.3390/app10197008

[25] Yu, Z., Shan, D. "An Experimental Study on Behaviour of Reinforced Concrete T-shaped Columns Subjected to Combined Loads", KSCE Journal of Civil Engineering, 25(3), pp. 906–919, 2021. https://doi.org/10.1007/s12205-021-0494-y

[26] Hsu, T. T. C. "Torsion of Structural Concrete – Plain Concrete Rectangular Sections", ACI Symposium Publication, 18, pp. 203–238, 1968.

[27] Hsu, T. T. C., Mo, Y. L. "Softening of Concrete in Torsional Members – Theory and Tests", ACI Journal Proceedings, 82(3), pp. 290–303, 1985. https://doi.org/10.14359/10335

[28] Solak, A. "Experimental Investigation of the Behavior of Reinforced Concrete Columns Under Axial Load and Torsional Effects", MSc Thesis, Konya Technical University, 2023.

[29] Timoshenko, S. P., Gere, J. M. "Theory of Elastic Stability", McGraw-Hill, 1961. ISBN 9780070647497

[30] Chen, S., Peng, W., Yan, W. "Experimental study on steel reinforced concrete columns subjected to combined bending–torsion cyclic loading", The Structural Design of Tall and Special Buildings, 27(11), e1479, 2018. https://doi.org/10.1002/tal.1479

[31] Li, Q., Belarbi, A. "Damage assessment of square RC bridge columns subjected to torsion combined with axial compression, flexure, and shear", KSCE Journal of Civil Engineering, 17(3), pp. 530–539, 2013. https://doi.org/10.1007/s12205-013-0600-x

[32] Prakash, S., Belarbi, A., You, Y.-M. "Seismic performance of circular RC columns subjected to axial force, bending, and torsion with low and moderate shear", Engineering Structures, 32(1), pp. 46–59, 2010. https://doi.org/10.1016/j.engstruct.2009.08.014

[33] Jiao, C., Liu, Y., Wei, B., Li, J., Hu, Z., Zhu, G. "Seismic performance of circular reinforced concrete columns subjected to compression, bending and torsion with low and moderate shear spanratio", Archives of Civil and Mechanical Engineering, 21(3), 135, 2021. https://doi.org/10.1007/s43452-021-00282-8

[34] TSE "TS 500/Şubat 2000 Betonarme Yapilarin Tasarim ve Yapim Kurallari" (Requirements for Design and Construction of Reinforced Concrete Structures), Turkish Standards Institution, Ankara, Türkiye, 2000. (in Turkish)

[35] Republic of Turkey Ministry of Environment and Urbanization. "Türkiye Bina Deprem Yönetmeligi – TBDY 2018" (Turkish Building Earthquake Code (TBEC 2018), Ankara, Türkiye, 2018. (in Turkish)

[36] Belarbi, A., Prakash, S., You, Y.-M. "Effect of spiral reinforcement on flexural-shear-torsional seismic behavior of reinforced concrete circular bridge columns", Structural Engineering and Mechanics, 33(2), pp. 137–158, 2009. https://doi.org/10.12989/sem.2009.33.2.137

[37] Solak, A., Cengiz, S., Ünal, A., Kamanli, M. "Numerical Investigation of Torsional Behaviour of Reinforced Concrete Elements with Different Section Shapes", Konya Journal of Engineering Sciences, 12(4), pp. 1022–1033, 2024. https://doi.org/10.36306/konjes.1536903

[38] BSI "BS EN 206:2013+A1:2016: Concrete — Specification, performance, production and conformity", British Standards Institution, Brussels, Belgium, 2016.

[39] BSI "BS EN 12390-3:2002: Testing hardened concrete — Part 3: Compressive strength of test specimens", British Standards Institution, Brussels, Belgium, 2002.

[40] BSI "BS EN 12390-5:2009: Testing hardened concrete — Part 5: Flexural strength of test specimens", British Standards Institution, Brussels, Belgium, 2009.

[41] Kaplan, S. A. "Betonarme Temel İlkeleri" (Reinforced Concrete Structure Elements), Teknik Yayınevi, 2004. (in Turkish) ISBN 9781111131180

[42] Yüksel, İ., Polat, Z. "Yield state investigation of reinforced concrete frames from a new point of view", Engineering Structures, 27(1), pp. 119–127, 2005. https://doi.org/10.1016/j.engstruct.2004.09.006

[43] Uğur, A. E., Ünal, A. "Assessing the structural behavior of reinforced concrete beams produced with macro synthetic fiber reinforced self-compacting concrete", Structures, 38, pp. 1226–1243, 2022. https://doi.org/10.1016/j.istruc.2022.02.051

[44] Dassault Systemes "ABAQUS/CAE, (2017)", [computer program] Available at: https://www.3ds.com/products/simulia/abaqus/cae [Accessed: 15 February 2026]

[45] Hussein, A., Marzouk, H. "Behavior of High-Strength Concrete under Biaxial Stresses", ACI Materials Journal, 97(4), pp. 27–36, 2000.

[46] Jankowiak, T., Lodygowski, T. "Identification of parameters of concrete damage plasticity constitutive model", Foundations of civil and environmental engineering, 6(1), pp. 53–69, 2005.

[47] Birtel, V., Mark, P. "Parameterised Finite Element Modelling of RC Beam Shear Failure", In: ABAQUS users' Conference, Cambridge, Massachusetts, United States,2006, pp. 95–108.

[48] International Federation for Structural Concrete "*fib* Model Code for Concrete Structures 2010", John Wiley & Sons, 2013. ISBN 9783433030615 https://doi.org/10.1002/9783433604090

[49] Paulay, T., Priestley, M. N. "Seismic Design of Reinforced Concrete and Masonry Buildings", Wiley, 1992. ISBN 9780471549154 https://doi.org/10.1002/9780470172841

[50] CEN "BS EN 1998-1:2004 Eurocode 8: Design of structures for earthquake resistance — Part 1: General rules, seismic actions and rules for buildings", European Committee for Standardization, Brussels, Belgium, 2005.